Brain Phenotypes in Two FGFR2 Mouse Models for Apert Syndrome

Kristina Aldridge,[1]* Cheryl A. Hill,[1] Jordan R. Austin,[1] Christopher Percival,[2] Neus Martinez-Abadias,[2] Thomas Neuberger,[3] Yingli Wang,[4] Ethylin Wang Jabs,[4] and Joan T. Richtsmeier[2]

Apert syndrome (AS) is one of at least nine disorders considered members of the fibroblast growth factor receptor (FGFR) -1, -2, and -3–related craniosynostosis syndromes. Nearly 100% of individuals diagnosed with AS carry one of two neighboring mutations on Fgfr2. The cranial phenotype associated with these two mutations includes coronal suture synostosis, either unilateral (unicoronal synostosis) or bilateral (bicoronal synostosis). Brain dysmorphology associated with AS is thought to be secondary to cranial vault or base alterations, but the variation in brain phenotypes within Apert syndrome is unexplained. Here, we present novel three-dimensional data on brain phenotypes of inbred mice at postnatal day 0 each carrying one of the two Fgfr2 mutations associated with AS. Our data suggest that the brain is primarily affected, rather than secondarily responding to skull dysmorphogenesis. Our hypothesis is that the skull and brain are both primarily affected in craniosynostosis and that shared phenogenetic developmental processes affect both tissues in craniosynostosis of Apert syndrome. *Developmental Dynamics 239:987–997, 2010.* © 2010 Wiley-Liss, Inc.

Key words: Apert syndrome; craniosynostosis; suture; mouse; skull; brain; development

Accepted 7 December 2009

INTRODUCTION

Apert syndrome (AS) is one of several genetic syndromes associated with craniosynostosis, occurring in 1 in 12.4–15.5/million live births (Cohen et al., 1992; Tolarova et al., 1997), with 99% of cases associated with one of two missense mutations in adjacent amino acids, Ser252Trp and Pro253Arg, of fibroblast growth factor receptor 2 (FGFR2). Individuals with AS display what has been described as a stereotypical constellation of dysmorphologies, most often including craniofacial dysmorphology and central nervous system (CNS) anomalies. However, the relative severity of brain dysmorphology and cognitive effects varies widely among individuals with AS (Blank, 1960; Lefebvre et al., 1986; Renier et al., 1996; Yacubian-Fernandes et al., 2004, 2005). Although an absence of alterations of brain morphology has been reported for some individuals diagnosed with AS (Yacubian-Fernandes et al., 2004, 2005), a large proportion of individuals display a range of neuroanatomical anomalies. These include increased intracranial volume (Gosain et al., 1995; Anderson et al., 2004), megalencephaly (Cohen and Kreiborg, 1990, 1991, 1994; Gosain et al., 1995; Posnick et al., 1995; Cohen, 2000), and ventriculomegaly (Tokumaru et al., 1996; Pooh et al., 1999; Cohen and MacLean, 2000; Renier et al., 2000; Yacubian-Fernandes et al., 2004; Quintero-Rivera et al., 2006). Other studies have observed dysmorphology of the corpus callosum (de Leon et al., 1987; Cohen

[1]Department of Pathology and Anatomical Sciences, University of Missouri-School of Medicine, Columbia, Missouri
[2]Department of Anthropology, Pennsylvania State University, University Park, Pennsylvania
[3]Huck Institutes of the Life Sciences, Pennsylvania State University, Hershey, Pennsylvania
[4]Department of Genetics and Genomic Sciences, Mount Sinai School of Medicine, New York, New York
Grant sponsor: NIH: NIDCR; Grant number: R01 DE018500.
***Correspondence to: Kristina Aldridge, Department of Pathology and Anatomical Sciences, University of Missouri-School of Medicine, One Hospital Drive, M309 Medical Sciences Building, Columbia, MO 65212.**
E-mail: aldridgek@health.missouri.edu

DOI 10.1002/dvdy.22218
Published online 13 January 2010 in Wiley InterScience (www.interscience.wiley.com).

and Kreiborg, 1990, 1991, 1994; Posnick et al., 1995), anomalies in limbic structure (de Leon et al., 1987; Cohen and Kreiborg, 1990, 1991; Renier et al., 2000; Quintero-Rivera et al., 2006), and in gyral patterning (Cohen and Kreiborg, 1990, 1991). Many individuals with AS display cognitive deficits, including mental retardation (Patton et al., 1988; Cohen and Kreiborg, 1990; Cohen, 2000); however, a large proportion of individuals with AS have an IQ well within the normal range (Patton et al., 1988; Yacubian-Fernandes et al., 2005), although other learning deficits may be present (Lefebvre et al., 1986). The nature of the association between phenotypic abnormalities and cognitive deficits is not known, but it has been shown that early surgical treatment of cranial dysmorphologies does not prevent mental deficiencies (Cohen and Kreiborg, 1990).

The wide diversity of brain phenotypes among individuals with AS has been attributed to various causes, including: secondary effects of the pattern of suture fusion (Cohen and Kreiborg, 1990; Yacubian-Fernandes et al., 2004), differing actions of the two FGFR2 mutations responsible for AS (Lajeunie et al., 1999), variation in penetrance and expressivity of the FGFR2 mutations (Passos-Bueno et al., 2008), and the potential differences in the action of the mutations on varying genetic backgrounds and environments (Slaney et al., 1996; Yacubian-Fernandes et al., 2005; Passos-Bueno et al., 2008). Theories about the variation in brain phenotypes in AS cannot be tested in humans, as the number of cases carrying each of the two mutations is not large enough to enable true genotype-phenotype correlations (Passos-Bueno et al., 2008), nor can environmental factors be easily accounted for in the study of humans. Thus, we turn to two inbred mouse models for AS on the same genetic background, the Apert syndrome $Fgfr2^{+/S252W}$ mouse (Wang et al., 2005) and the Apert syndrome $Fgfr2^{+/P253R}$ mouse (Wang et al., in press) to compare the effects of the two AS genetic mutations on brain phenotypes.

Mice with the Fgfr2 S252W mutation have been shown to display reduced body size and craniofacial dysmorphology that mirrors that described in individuals with AS, including coronal suture fusion and metopic defect of the skull (Chen et al., 2003; Wang et al., 2005). Adult $Fgfr2^{+/P253R}$ mice have also been shown to display AS-like phenotypes, including craniofacial dysmorphology, coronal suture fusion, limb abnormalities, and abnormalities of skull osteogenesis and chondrogenesis (Yin et al., 2008; Wang et al., in press).

Fibroblast growth factors induce diverse cellular responses in multiple biological systems by binding to high-affinity cell-surface receptors suggesting their function as morphogens during development (Hughes, 1997). FGFR2 signaling is known to regulate stem cell proliferation, affecting different cell lineages. The affected lineages include those important to the control of endochondral and intramembranous bone formation in cranial and postcranial structures (Iseki et al., 1999; Eswarakumar et al., 2002a), and those critical to the developing CNS, as indicated by expression local to the neural tube during neural crest cell migration, and in branchial arches following neural crest cell migration (Wilke et al., 1997). Given the exquisite regulation of Fgfr activity (Hughes, 1997; Ornitz and Marie, 2002), subtle variations in tissue-specific patterns of FGFR expression may be responsible for the complex patterning of normal morphogenetic processes like angiogenesis and bone formation, as well as the dysmorphogenetic mechanisms underlying conditions like Apert syndrome. An appreciation for the complexity of FGF–FGFR interactions shows that the two known mutations that cause Apert syndrome could produce varying patterns and magnitudes of phenotypic effects on many developing systems, including the CNS.

To date, there has been no comparison of the effects of either of the two mutations on brain morphology. This study is the first investigation of brain morphology in mouse models for AS and the first to compare the phenotypic effects of each mutation on the brain. In this study, we compare brain phenotypes among inbred $Fgfr2^{+/S252W}$, $Fgfr2^{+/P253R}$, and their wild-type littermates with the C57BL/6J strain at postnatal day (P) 0 using data from three-dimensional (3D) magnetic resonance microscopy (MRM) and morphometric methods. By studying mice on the day of birth we reduce the effect of external environmental factors that influence patterns of postnatal growth.

RESULTS

Brain Size in $Fgfr2^{+/S252W}$ and $Fgfr2^{+/P253R}$ Mice

MRM images were acquired of all mice at the High Field Magnetic Resonance Facility of the Huck Institutes of the Life Sciences at the Pennsylvania State University (http://www.huck.psu.edu/facilities/hf-magnetic-resonance-up). The 3D coordinate locations of neuroanatomical landmarks were recorded for 45 mice (ten $Fgfr2^{+/S252W}$ and 11 of their wild-type littermates, and 14 $Fgfr2^{+/P253R}$ and ten of their wild-type littermates) from MRM images using Analyze 9.0 (Robb et al., 1989). Fifteen landmarks (five bilateral, five midline) were defined for internal and surface cerebral, midbrain, cerebellar, and brainstem structures (Table 1; Fig. 1). Overall brain size, estimated as the geometric mean of all possible linear distances between these landmarks (Darroch and Mosimann, 1985; Falsetti et al., 1993) was statistically compared among mutant and wild-type groups using Mann-Whitney U tests (Mann and Whitney, 1947). Of the four groups compared, average brain size is largest in $Fgfr2^{+/S252W}$ mice (Table 2; Fig. 2). Average brain size of $Fgfr2^{+/S252W}$ mice exceeds that of wild-type mice and of $Fgfr2^{+/P253R}$ mice in this sample. Average brain size is similar in $Fgfr2^{+/P253R}$ mice and wild-type mice.

Coronal Suture Fusion in Apert Syndrome $Fgfr2^{+/S252W}$ and $Fgfr2^{+/P253R}$ Mice

μ-Computed tomography (μ-CT) images were acquired at the Center for Quantitative Imaging at the Pennsylvania State University (www.cqi.psu.edu) and reconstructed in three dimensions to visualize and assess cranial suture patency in $Fgfr2^{+/S252W}$ mice and their wild-type littermates, and $Fgfr2^{+/P253R}$ mice and their wild-type littermates. None of the wild-type mice display fusion of any cranial vault suture at P0. On the other hand,

TABLE 1. Anatomical Definitions of 15 Three-Dimensional Brain Landmarks Collected From MRM Images of Mice at P0[a]

Landmark (left, right)	Anatomical definition	Midline (M) Bilateral (B)	Cerebrum (C) Cerebellum (Cb) Brainstem (Br)
1,2	Most superolateral point of intersection of olfactory bulb with anterior frontal lobe surface	B	C
3,4	Most caudolateral point on occipital lobe surface	B	C
5	Most caudal point on cerebellar surface	M	Cb
6,7	Most lateral point on cerebellar surface	B	Cb
8,9	Centroid of head of caudate nucleus	B	C
10,11	Origin of middle cerebral artery from Circle of Willis on ventral cerebral surface	B	C
12	Genu of corpus callosum	M	C
13	Anterior commissure	M	C
14	Splenium of corpus callosum	M	C
15	Intersection of pons with most caudal aspect of the ventral cerebral surface	M	Br

[a]Landmarks are illustrated in Figure 1.

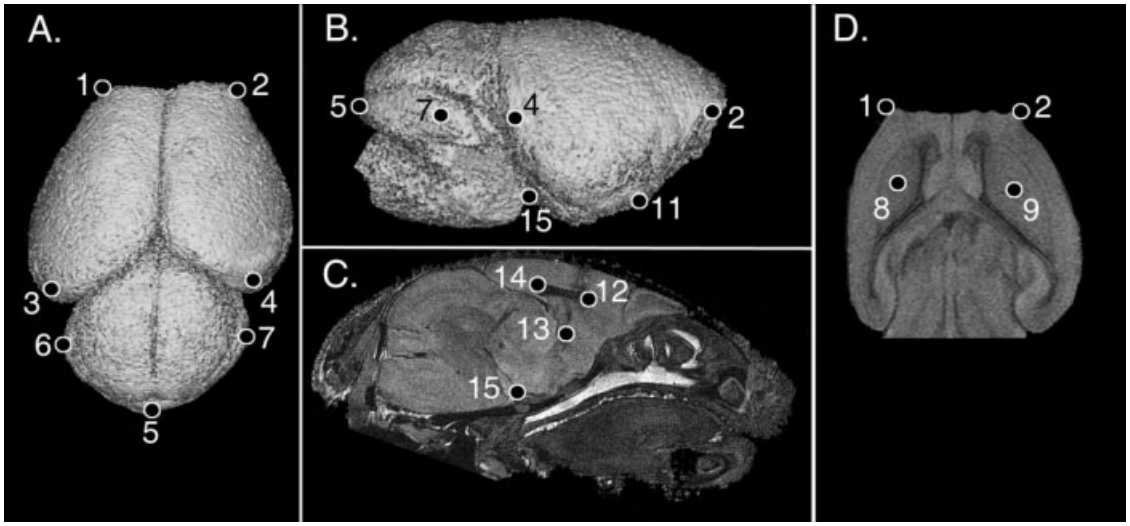

Fig. 1. Landmarks collected from magnetic resonance microscopy (MRM) images of postnatal day (P) 0 mouse brains illustrated on three-dimensional (3D) reconstructions of the MRM images. **A**: Dorsal view. **B**: Lateral view of right side. **C**: Midsagittal view. **D**: Axial slice. Landmark definitions are in Table 1.

results show clear variation in both pattern and degree of coronal suture closure in the mutant mice of both models at P0 (Martinez-Abadias et al., in preparation). $Fgfr2^{+/S252W}$ and $Fgfr2^{+/P253R}$ mice are observed with fusion of the right coronal suture, the left coronal suture, and of both coronal sutures (Table 3). Importantly, these varying patterns of suture closure are observed within litters of mice.

Of the 10 $Fgfr2^{+/S252W}$ mice, 7 display complete fusion of both coronal sutures, and 3 display complete unilateral coronal fusion. Of the three mice with unilateral suture fusion, two of them display partial fusion of the contralateral coronal suture, with the remaining mouse having one patent coronal suture. Of the 14 $Fgfr2^{+/P253R}$ mice, 6 display complete fusion of the left and right coronal sutures, 2 display partial fusion of both coronal sutures, and 6 display complete unilateral fusion of the coronal suture. Of the six mice with unilateral fusion, three display partial fusion of the contralateral coronal suture and three display patency of the contralateral coronal suture.

Brain Morphology Phenotype in $Fgfr2^{+/S252W}$ and $Fgfr2^{+/P253R}$ Mice

MRM images were reconstructed in 3D to visualize and assess the gross morphology of the brain. All non-neural tissues (e.g., skull, dura, blood vessels), as well as the olfactory bulbs were removed from the MRM images using Analyze 9.0 (Robb et al., 1989) to reconstruct the brain surface. From these reconstructions, we qualitatively assessed overall brain morphology, brain symmetry, gross defects of

the corpus callosum, and ventriculomegaly of the lateral ventricles and fourth ventricle. Results of these observations are presented in Table 3 and example phenotypes are illustrated in Figure 3.

Brain morphology in Fgfr2$^{+/S252W}$ mice is highly variable. Although all Fgfr2$^{+/S252W}$ mice show reduced brain length (rostrocaudal) and increased cerebral height (dorsoventral), the magnitude of these effects varies considerably among the mutant mice. Additionally, the severity of cerebral asymmetry in each individual is variable. Of the 10 Fgfr2$^{+/S252W}$ mice, 4 mice display severe asymmetry and 1 mouse is mildly asymmetric, with the remaining 5 mice showing no obvious asymmetry. Size of the lateral ventricles does not appear to differ between mutant and wild-type mice (i.e., there is no obvious ventriculomegaly of lateral ventricles), although two mice displayed enlarged fourth ventricles. Two of the ten Fgfr2$^{+/S252W}$ mice display a distinctly arched corpus callosum. These patterns of observable brain morphology are not obviously associated with particular patterns of coronal suture fusion. For example, a mouse with both coronal sutures fused

TABLE 2. Sample Sizes and Results of Mann-Whitney U Tests Comparing Brain Size Among Fgfr2$^{+/S252W}$, Fgfr2$^{+/P253R}$, and Wild-Type Littermates

	Brain size (Mean % difference, P value)
Fgfr2$^{+/S252W}$ (N=8) vs. WT (N=11)	101.8% $P = 0.041$
Fgfr2$^{+/P253R}$ (N=14) vs. WT (N=8)	100.00% $P = 0.953$
Fgfr2$^{+/S252W}$ vs. Fgfr2$^{+/P253R}$	101.1% $P = 0.160$

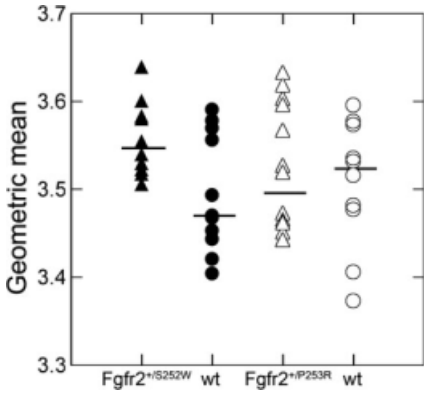

Fig. 2. Comparisons of brain size as measured by the geometric mean of all possible linear distances among Fgfr2$^{+/S252W}$, Fgfr2$^{+/P253R}$, and wild-type littermates. Closed triangles, Fgfr2$^{+/S252W}$; open triangles, Fgfr2$^{+/P253R}$; circles, wild-type (wt) littermates. Bars = median values.

TABLE 3. Coronal Suture Patency and Brain Phenotypes in Apert Syndrome Fgfr2$^{+/S252W}$ and Fgfr2$^{+/P253R}$ Mice, and Wild-Type Littermate Mice at P0[a]

Mouse ID	Right coronal suture	Left coronal suture	Degree of overall asymmetry	Corpus callosum shape	Lateral ventricle enlargement	Fourth ventricle enlargement
Fgfr2$^{+/S252W}$ N=10						
A	**F**	**F**	**Mild**	Normal	Normal	**Large**
B	**F**	P	None	Normal	Normal	Normal
C	**F**	**F**	**Severe**	Normal	Normal	Normal
D	**F**	**F**	**Severe**	**Arched**	Normal	Normal
E	**F**	O	**Severe**	Normal	Normal	Normal
F	**F**	**F**	**Severe**	Normal	Normal	Normal
G	P	**F**	None	Normal	Normal	Normal
H	**F**	**F**	None	**Arched**	Normal	Normal
I	**F**	**F**	None	**Normal**	Normal	Normal
J	**F**	**F**	None	**Normal**	Normal	**Large**
Fgfr2$^{+/P253R}$ N=14						
a	P	**F**	**Severe**	Normal	**Large**	Normal
b	P	P	**Mild**	Normal	Normal	Normal
c	**F**	P	None	Normal	Normal	Normal
d	O	**F**	None	Normal	Normal	Normal
e	**F**	O	None	Normal	Normal	**Large**
f	**F**	**F**	None	**Arched**	Normal	Normal
g	**F**	**F**	None	**Arched**	Normal	**Large**
h	P	**F**	None	Normal	Normal	Normal
i	**F**	**F**	None	Normal	Normal	Normal
j	**F**	**F**	None	**Arched**	Normal	Normal
k	**F**	**F**	None	Normal	Normal	Normal
l	**F**	**F**	None	Normal	Normal	Normal
m	P	P	None	Normal	Normal	Normal
n	O	**F**	None	Normal	Normal	Normal

[a]O indicates less than 25% of the length of the suture is fused; P, greater than 25% but less than 75% of the length of the suture is fused; F, more than 75% of the length of the suture is fused. Example phenotypes are illustrated in Figure 3.

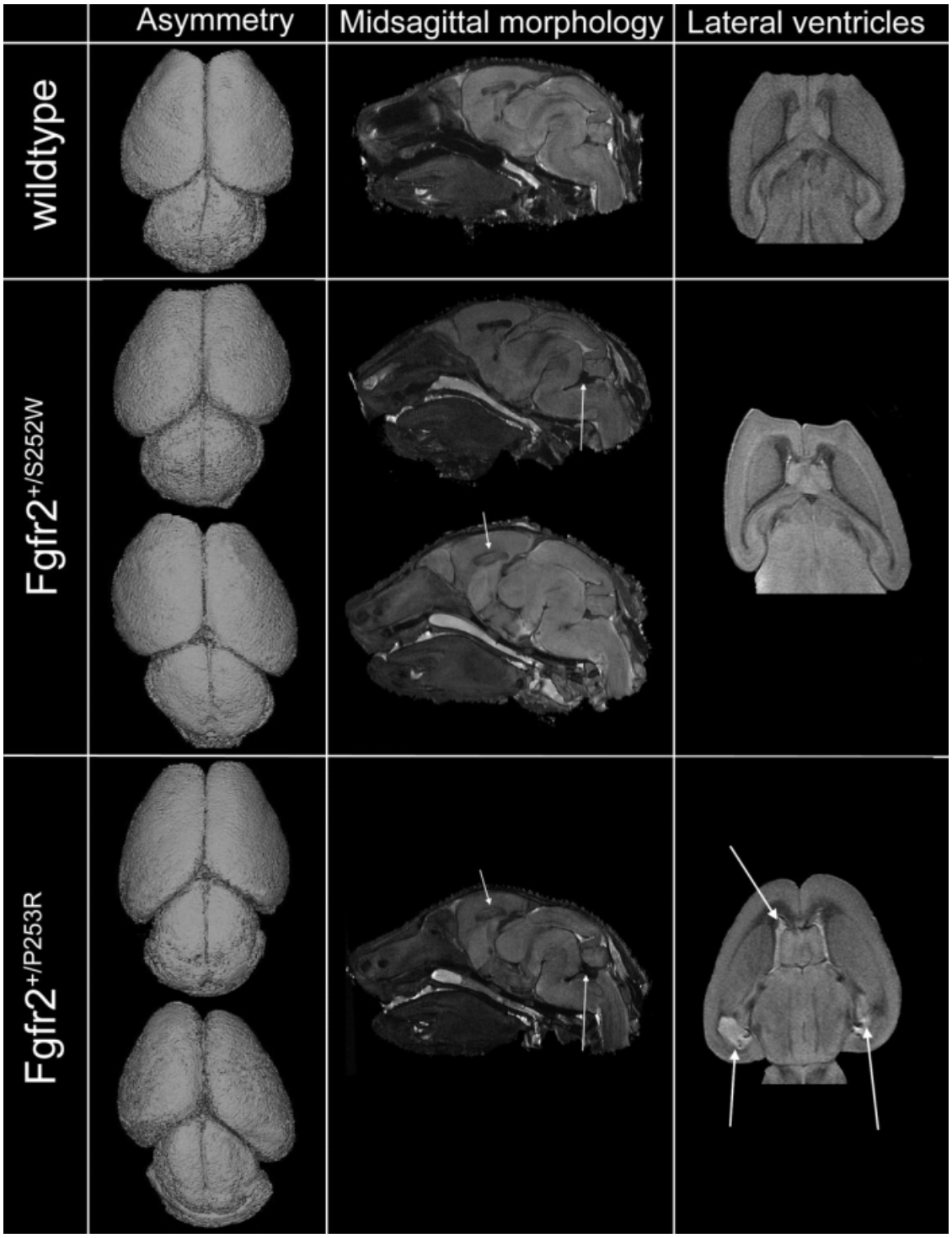

Fig. 3. Three-dimensional reconstructions of superior surfaces (first column), midsagittal planes (second column), and axial slice images (last column) of magnetic resonance microscopy (MRM) data, illustrating examples of variation in brain phenotypes. Row 1: Wild-type mouse. Row 2: $Fgfr2^{+/S252W}$ mice with slight cerebral asymmetry (above) and severe cerebral asymmetry (below), enlarged fourth ventricle (above, white arrow) and arched corpus callosum (below, white arrow), and unremarkable lateral ventricles. Row 3: $Fgfr2^{+/P253R}$ mice with slight cerebral asymmetry (above) and severe cerebral asymmetry (below), enlarged fourth ventricle and arched corpus callosum (white arrows) and enlarged lateral ventricles (white arrows).

may appear as asymmetric as a mouse with unilateral fusion.

As observed in the $Fgfr2^{+/S252W}$ mice, many of the $Fgfr2^{+/P253R}$ mice display relatively reduced rostrocaudal length and increased dorsoventral height of the cerebrum, but the severity of these differences are variable. Furthermore, there is severe cerebral asymmetry in 1 of the mutant mice and mild asymmetry in another, with the remaining 12 mice displaying

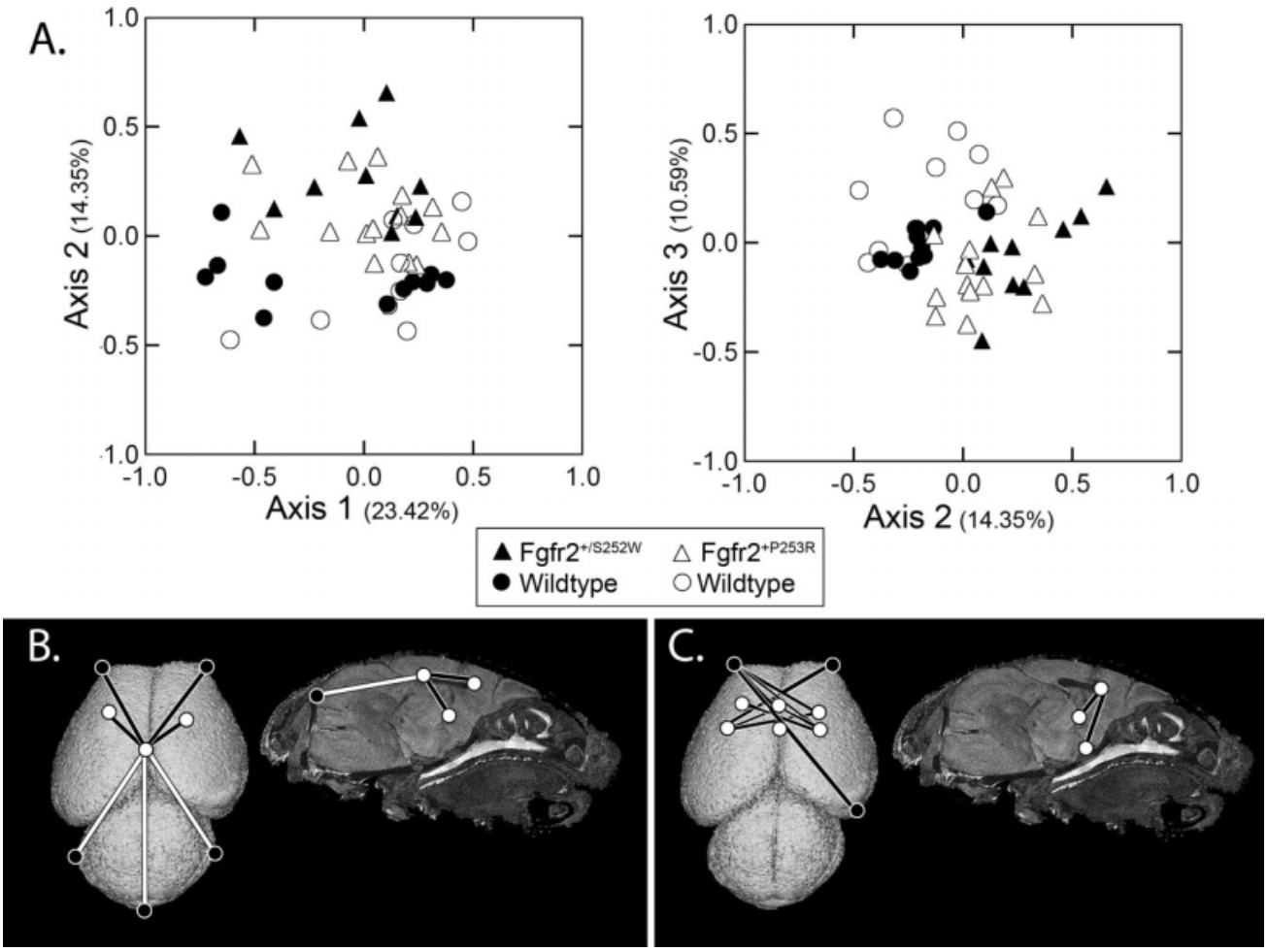

Fig. 4. Results of PCOORD analyses of landmark coordinate data collected from brain structures, including $Fgfr2^{+/S252W}$, $Fgfr2^{+/P253R}$, and wild-type littermate mice. **A**: Eigenscores plotted for the first three principal axes and the percent of variation accounted for by each axis. Closed triangles, $Fgfr2^{+/S252W}$ mice; open triangles, $Fgfr2^{+/P253R}$ mice; circles, respective wild-type littermates. **B**: Linear distances strongly positively correlated with Axis 1. **C**: Linear distances strongly correlated with Axis 2. Black lines, strong positive correlations; white lines, strong negative correlations. Black dots, landmarks located in plane of view; white dots, landmarks deep to the plane of view.

overall symmetry of the cerebral hemispheres. Of the 14 $Fgfr2^{+/P253R}$ mice, 3 display a markedly arched corpus callosum in the midline, although the relative severity of the angle is variable, as is the relative superoinferior thickness of the midline aspect of this structure. Of the 14 mice, 2 also appear to have an enlarged fourth ventricle, and one mouse displays enlarged lateral ventricles. As seen in $Fgfr2^{+/S252W}$ mice, the patterns of observable brain morphology in $Fgfr2^{+/P253R}$ are not obviously associated with a particular pattern of coronal suture fusion.

Quantitative Comparisons of Brain Phenotypes

We quantitatively assessed brain morphology using a principal coordinates application of Euclidean distance matrix analysis, or PCOORD (Lele and Richtsmeier, 2001). Principal coordinates analysis (PCOORD) allows determination of the specific combination of morphological variables that successfully separate individuals into groups of known membership by measuring dissimilarity among individuals within a multidimensional "form space" (Richtsmeier et al., 1998). A series of orthogonal axes are fitted into the form space accounting for the majority of the variation among cases. The ordination of individuals along these axes indicates morphological groupings among the mice based on commonalities of combinations of metric variables. Examination of variables that are strongly correlated with the principal axes reveals those variables that account for the most variation between groups. Results of PCOORD analyses of the landmark data representing brain morphology of all mice (Fig. 4) show that the first and third principal axes (accounting for 23.42% and 10.59% of variance, respectively) do not reveal distinct subgroups based on model or genotype. In contrast, the second principal axis (14.35% of variance) shows both groups of wild-type mice clustering primarily on the negative end of the axis while the mice carrying the FGFR2 mutations are located on the positive end. Linear distances that are strongly correlated with position along this 2nd principal axis describe an increased superoinferior height of the cerebrum and increased breadth of the rostral cerebrum in both groups of mutant mice

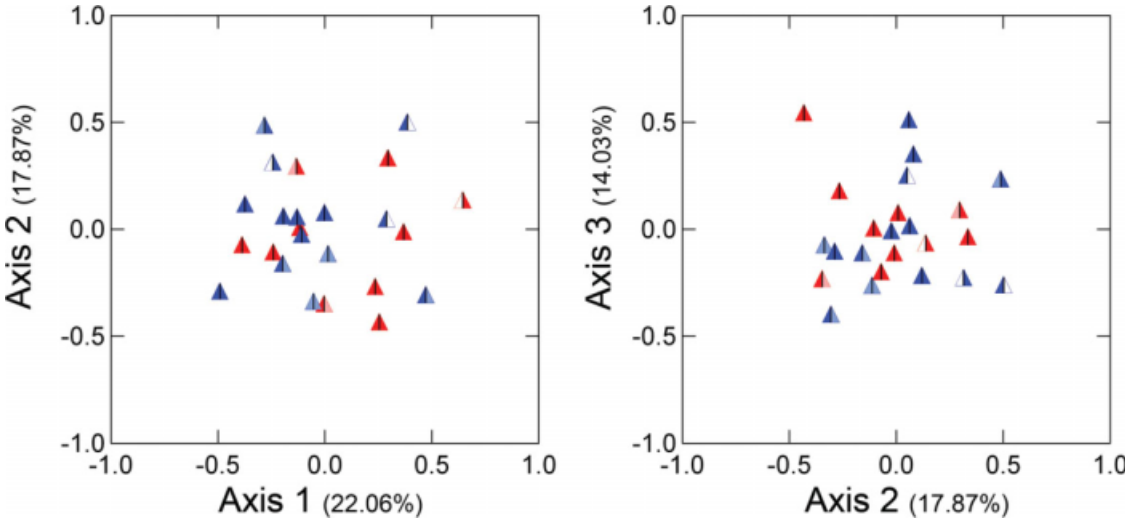

Fig. 5. Results of PCOORD analyses of landmark coordinate data collected from brain structures, including only Fgfr2$^{+/S252W}$ (red triangles) and Fgfr2$^{+/P253R}$ (blue triangles) mice. Eigenscores plotted for the first three principal axes and the percent of variation accounted for by each axis. Darkness of each half of the symbols indicate the pattern of coronal suture fusion for that individual (left–right), where dark blue/red indicate complete fusion, light blue/red indicate partial fusion, and white = patent suture.

relative to wild-type. When PCOORD analysis is conducted using only Fgfr2$^{+/S252W}$ and Fgfr2$^{+/P253R}$ (Fig. 5) no distinct clusters of individuals are revealed along any of the first three principal axes (55.03% of variance, collectively) based on genotype, nor do individuals form clusters based on pattern of cranial suture fusion. These results suggest that despite small differences in overall brain size, brain morphology does not distinguish Fgfr2$^{+/S252W}$ from Fgfr2$^{+/P253R}$ mice, or distinguish mice with varying patterns of suture fusion.

DISCUSSION

Brain Size Is Not Increased in Either Model at P0

One of the most often noted characteristics of individuals with AS is increased intracranial volume (ICV; Gosain et al., 1995; Posnick et al., 1995; Anderson et al., 2004). However, it has also been noted that ICV is in the normal range at birth with rapid postnatal increase (Gosain et al., 1995). A study comparing the two AS mutations in humans determined that there is no difference in ICV (Anderson et al., 2004). The P0 mice carrying the FGFR2 mutations in this study show slightly larger brain size relative to their normal littermates. Additionally, as observed in AS, there was no significant difference in brain size between the groups carrying the different Fgfr2 mutations. Analyses of these mouse models of AS at later developmental stages are required to determine whether brain size or ICV is increased postnatally as is observed in AS.

Patterns of Gross Brain Morphology Are Highly Variable in Fgfr2$^{+/S252W}$ and Fgfr2$^{+/P253R}$ Mice

Severity of CNS abnormalities varies considerably among individuals with AS (Blank, 1960). CNS anomalies have been observed in 55.6% of individuals with AS in a study by Yacubian-Fernandes and colleagues (2005). However, CNS anomalies were not observed in 25% of AS individuals studied by Renier et al (2000), 28% studied by Renier et al. (1996), and 44.4% studied by Yacubian-Fernandes et al (2004). Only one anomaly was observed in 16.7% of the individuals with AS in the latter study. Of the 10 Fgfr2$^{+/S252W}$ mice, 3 did not show any CNS abnormalities (30%), and 5 showed only one abnormality (50%). Of the 14 Fgfr2$^{+/P253R}$ mice, 8 showed no CNS abnormalities (57%), and 4 mice displayed a single anomaly (29%). No brain anomalies were observed in the wild-type mice.

In Fgfr2$^{+/S252W}$ mice, the most frequently observed anomaly is asymmetry of cerebral hemispheres, while only two of the Fgfr2$^{+/P253R}$ mice showed asymmetry. However, the presence and the severity of cerebral asymmetry do not correlate with the pattern of coronal suture fusion. Overall brain morphology in AS has been described as often asymmetric (Fig. 6), although the degree of asymmetry varies (Lefebvre et al., 1986). The relationship between cerebral asymmetry and coronal suture fusion has not been systematically investigated in humans.

Ventriculomegaly is often observed in humans with AS (Noetzel et al., 1985; Cohen and Kreiborg, 1990, 1994) and increased size of the lateral ventricles has been observed in various frequencies in individuals with AS. For example, Yacubian-Fernandes et al. (2004) observed ventriculomegaly in 27.8% of individuals with AS in their study, Renier et al. (1996) observed it in 43% of AS individuals studied, and Quintero-Rivera et al. (2006) observed 89% of AS individuals with ventriculomegaly. Noetzel et al. (1985) provide a developmental consideration of ventriculomegaly and state that when it is present at birth in individuals with AS, it does not progress with postnatal development or change postoperatively. They suggest that the ventriculomegaly results from a primary disturbance of embryologic development, rather than occurring secondary to abnormal skull development. Only one of the

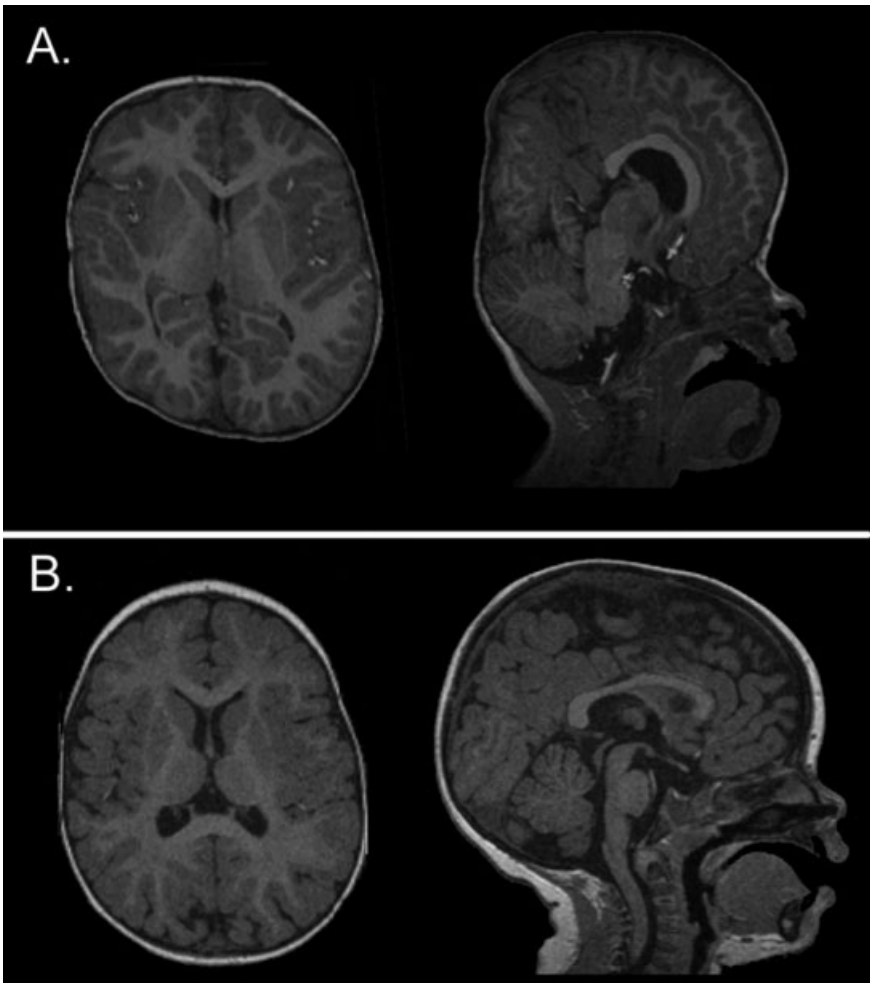

Fig. 6. **A,B**: Example MRIs of a child with AS (A) and a typically developing child (B). Cerebral asymmetry is observed in the axial plane of A (left image) as compared to B. The frequently observed arched corpus callosum is observed in the sagittal plan of A (right image). Compare with arched corpus callosum in Fgfr2$^{+/S252W}$ and Fgfr2$^{+/P253R}$ mice illustrated in Figure 3.

mice in our study displayed enlarged lateral ventricles (Fgfr2$^{+/P253R}$), although four mice were observed to have enlarged fourth ventricles (two Fgfr2$^{+/S252W}$ and two Fgfr2$^{+/P253R}$). The difference in this trait between mice and humans with AS may be due to species-specific differences in brain composition. Further study of this trait is necessary to determine the cause for the divergent findings.

Many individuals with AS show dysmorphology of the corpus callosum (Cohen and Kreiborg, 1990, 1993), but it has been observed as normal in up to 70% of AS individuals considered in other studies (Renier et al., 1996; Yacubian-Fernandes et al., 2004). Dysmorphology of the corpus callosum in individuals with AS is observed on the midsagittal plane as arched or rounded as compared to a more anteroposteriorly elongated and flat structure in typically developing individuals (Fig. 6). Two of the Fgfr2$^{+/S252W}$ and three Fgfr2$^{+/P253R}$ mice in this study show the rounded corpus callosum (Fig. 3). This indicates a similar proportion of mice with the two FGFR2 mutations that show a rounded corpus callosum shape, which is similar to the proportion observed in individuals with AS.

3D Quantitative Brain Phenotypes Mirror Those Observed in AS

Marsh et al. (1991) described the shape of the head in AS as having a flat and elongated forehead, broader bitemporal width, broad and flattened occipital regions, and anteroposteriorly shortened cranial lengths. Cohen and Kreiborg (1994) describe dramatic increases in head height and decreased head length present at birth. Additionally, they describe the decrease in head length as more pronounced than the observed increase in head breadth. Although our gross observations showed a distinction between both mutant models and their respective littermates in the rostrocaudal length of the cerebrum and the overall brain as described for humans with AS, the quantitative traits that most strongly distinguish mutant from wild-type mice were the mediolateral breadth of the rostral cerebrum and overall dorsoventral cerebral height. Many studies of brain morphology in individuals with AS include children of older ages, suggesting this trait may become exacerbated later in postnatal development. Study of later development in these mice will shed light on this possibility. Indeed, Yin et al. (2008) and Wang et al. (2005, in press) described decreased cranial length, increased cranial height and increased cranial width between paired frontal bones in the skulls of adult Fgfr2$^{+/P253R}$ mice, suggesting this may be the case. Because, to our knowledge, there have not been quantitative analyses of 3D brain morphology of children with AS, it is difficult to directly compare our results with the human condition.

Brain Phenotypes Are Similar in Fgfr2$^{+/S252W}$ and Fgfr2$^{+/P253R}$ Mice

Although clear differences exist in the phenotypic effects of the two Fgfr2 mutations on brain phenotypes at P0, our results do not support a hypothesis of one mutation showing relatively more severe effects. Brain size is significantly increased in Fgfr2$^{+/S252W}$ mice by slightly less than 2%. In comparison, mean Fgfr2$^{+/P253R}$ brain size is increased by more than 1% relative to wild-type littermates, although this difference is not statistically significant. Additionally, a greater proportion of Fgfr2$^{+/S252W}$ mice display cerebral asymmetry than observed in Fgfr2$^{+/P253R}$. Significantly, overall brain morphology distinguishes each AS mouse model from their respective

wild-type littermates, but does not distinguish the two Apert mouse models from one another.

Brain Anomalies at P0 Are Not Correlated With Patterns of Suture Fusion

It has been suggested that CNS anomalies in AS are the result of cranial suture fusion (Cohen and Kreiborg, 1990; Yacubian-Fernandes et al., 2004). The results of our study do not support this hypothesis. We find no evidence of correspondence between the pattern of suture fusion/patency and both qualitative and quantitative brain phenotypes, including cerebral asymmetry, corpus callosum dysmorphology, and overall brain morphology. These findings suggest a degree of independence in the processes underlying phenotypic alterations of calvarial vault sutures and brain dysmorphogenesis.

There are several potential explanations for our findings. Remembering that we are looking only at P0 mice, one possibility is that the mutations in FGFR2 have independent effects on formative tissues (neurogenic vs. chondrogenic vs. osteogenic), and that these effects produce early alterations in morphogenesis of each tissue which in turn can ultimately affect the formation of alternate tissues. FGFR2 is expressed in the developing neural tube in proliferating neuronal precursor cells (Maric et al., 2007; Frinchi et al., 2008). It is also expressed throughout the neural tube during neural crest cell migration (Wilke et al., 1997). Expression of FGFR2 increases with age in certain regions of the brain, including white matter of the cerebrum and cerebellum (Bansal et al., 2003). Alternatively, the mutations in FGFR2 may have an effect on a third tissue that then affects both neural and osteogenic tissues. For example, a thin layer of neural crest cell-derived cells travels with developing cerebral hemispheres, ultimately developing into the mature meningeal tissues (Gagan et al., 2007), a tissue that has been proposed to be involved in the production of craniosynostosis phenotypes (Moss and Young, 1960; Moss, 1979, 1997a–d; Opperman et al., 1993, 1995, 1998).

A second possibility is that suture fusion patterns may show a recognizable relationship with brain morphology at later developmental stages that is not observed at P0. The continued integration of various tissues during postnatal growth may produce increased correlations between suture fusion, skull dysmorphology, and brain phenotypes. Previous work on brain morphology in human infants with isolated, single-suture craniosynostosis has shown patterns of brain morphology in infancy that correlate with skull dysmorphology (Gault et al., 1992; Aldridge et al., 2002, 2005, 2006; Richtsmeier et al., 2006). Study of infants with isolated, single-suture sagittal synostosis 1 year following surgical alteration of the calvarial vault also showed postoperative changes in brain morphology (Aldridge et al., 2005). However, studies have also shown patterns of brain dysmorphology, both pre- and postoperatively, that cannot be explained by the shape of the skull (Aldridge et al., 2002, 2005, 2006). These studies have included infants several months postnatal, not at birth as in the present study of P0 mice. Future investigation of brain shape, skull shape, and suture biology in mouse models of Apert syndrome at postnatal time points will determine whether brain morphology can be predicted by calvarial vault suture fusion patterns at later ontogenetic stages despite the lack of correlation at birth.

CONCLUSIONS

Enormous progress has been made in identifying various mutations associated with the production of craniosynostosis. Still, even for those cases in which a causal gene has been defined, the precise role of this mutation in producing craniofacial dysmorphology is unidentified. The gap between molecular events and phenotype obscures our understanding of disease process, prevents an accurate prediction of individual phenotypes, and precludes the design of individualized therapeutic strategies.

FGFR1, FGFR2, and FGFR3 tyrosine kinases and their ligands are known to play a crucial role in the control of cell migration, proliferation, differentiation, and survival by activating two primary pathways (Ornitz and Itoh, 2001; Wang et al., 2006). Signaling through FGFR2 is known to regulate stem cell proliferation, affecting multiple cell lineages including those important to brain and bone formation (Iseki et al., 1999; Eswarakumar et al., 2002b). Simultaneous expression of Fgf ligands at sites in brain and skull primordia in an organism with an Fgfr mutation will result in abnormal cellular function local to those sites. The abnormal cellular processes experienced by these separate tissues will initiate a series of events that result in local sites of dysmorphogenesis that are ultimately observed as a composite phenotypic outcome.

We have demonstrated anomalies of the developing brain in two Fgfr2 models for Apert syndrome, and our data suggest little or no relationship between patterns of premature suture closure and brain dysmorphology at P0. Further dissection of the co-development of skull and brain morphology will define change in local developmental processes that underlie craniosynostosis phenotypes and their variation. The developmental relationships between these two important tissues are key to the elucidation of the genotype-phenotype continuum in craniosynostosis.

EXPERIMENTAL PROCEDURES

Generation of Targeting Construct and Mutant Mice

The Apert $Fgfr2^{+/S252W}$ and $Fgfr2^{+/P253R}$ mice were generated in the laboratory of Dr. Ethylin Wang Jabs (Wang et al., 2005, in press). They were consistently inbred to a C57BL/6J background to minimize phenotypic variation due to genetic differences. Genotyping of tail DNA to distinguish mutant from wild-type progeny was carried out by polymerase chain reaction analysis. The primers for Fgfr2 were as described (Wang et al., 2005). Care and use of mice for this study were in compliance with the relevant animal welfare guidelines approved by the Johns Hopkins University Animal Care and Use Committee and the Mount Sinai School of Medicine Animal Care and

Use Committee. Mice were killed on P0 by inhalation anesthetics and weighed. The carcasses were fixed and heads were perfused in 4% paraformaldehyde. Our sample consists of $Fgfr2^{+/S252W}$ (N = 10) and their wild-type littermates (N = 11), and $Fgfr2^{+/P253R}$ (N = 14) and their wild-type littermates (N = 10).

MRM and μ-CT Imaging Protocols

The fixed animals were immersed in a 2% Magnevist (Bayer Health Care, Wayne, NJ) phosphor-buffered solution for 10 days to reduce the T1 and T2 relaxation times. The achieved short T1 (32 ms) and T2 (8 ms) times allowed for fast imaging with a high contrast-to-noise ratio. To prevent the animals from drying out and to minimize magnetic susceptibility artifacts during scanning the specimens were surrounded by a flourinert liquid FD-43 (3M, St. Paul, MN). All experiments were conducted on a vertical 14.1 Tesla Varian (Varian Inc., Palo Alto, CA) imaging system with direct drive technology. A home-built loop gap resonator with a diameter of 2.0 cm was used to acquire standard three-dimensional spin echo images of the head of the animal. Images up to an isotropic resolution of 40 μm were acquired. A standard imaging experiment with an isotropic resolution of 80 μm comprised a field of view of 15.4 × 14 × 11 mm^3 and a matrix size of 192 × 132 (75% partial Fourier: 176) × 137. With eight averages and a repetition time of 75 ms (echo time 25 ms) the total scan time was three hours. Matlab (The MathWorks, Inc., Natick, MA) was used for postprocessing. By zero-filling each direction by a factor of two the pixel resolution of the standard imaging experiment was 40 μm^3.

μ-CT images were acquired at the Center for Quantitative Imaging at the Pennsylvania State University (www.cqi.psu.edu) using the HD-600 OMNI-X high-resolution X-ray computed tomography system (Bio-Imaging Research Inc, Lincolnshire, IL) following already established protocols (Parsons et al., 2007; Hill et al., 2007) with pixel size of 0.15–0.02 mm and 0.15–0.025 mm slice thickness.

Landmark Data Collection and Analysis

Anatomical landmarks represent biologically meaningful points that can be repeatedly located with a high degree of accuracy and precision (Richtsmeier et al., 1995). Landmarks are illustrated in Figure 1 and defined in Table 1. Precision of landmark data collection was evaluated following previously described methods (Aldridge et al., 2007). After checking for gross errors of landmark placement, data from the two trials were averaged to minimize intra-observer error.

ACKNOWLEDGMENTS

The authors thank Dr. Tim Ryan at the Center for Quantitative Imaging for his work in obtaining μ-CT images of the mice. This manuscript benefited from the thoughtful comments of two anonymous reviewers. Work was supported in part by funds from the Department of Pathology and Anatomical Sciences at the University of Missouri.

REFERENCES

Aldridge K, Marsh J, Govier D, Richtsmeier J. 2002. Central nervous system phenotypes in craniosynostosis. J Anat 201:31–39.

Aldridge K, Kane A, Marsh J, Panchal J, Boyadijiev S, Yan P, Govier D, Ahmad W, Richtsmeier J. 2005. Brain morphology in nonsyndromic unicoronal craniosynostosis. Anat Rec 285:690–698.

Aldridge K, Kane A, Marsh J, Yan P, Govier D, Richtsmeier J. 2006. Relationship of brain and skull in pre- and postoperative sagittal synostosis. J Anat 206: 373–385.

Aldridge K, Reeves R, Olson L, Richtsmeier J. 2007. Differential effects of trisomy on brain shape and volume in related aneuploid mouse models. Am J Med Genet Part A 143A:1060–1070.

Anderson P, Netherway D, Abbott A, Cox T, Roscioli T, David D. 2004. Analysis of intracranial volume in Apert syndrome genotypes. Pediatr Neurosurg 40:161–164.

Bansal R, Lakhina V, Remedios R, Tole S. 2003. Expression of FGF receptors 1, 2, 3 in the embryonic and postnatal mouse brain compared with Pdgfra, Olig2 and Plp/dm20: implications for oligodendrocyte development. Dev Neurosci 25: 83–95.

Blank C. 1960. Apert's syndrome (a type of acrocephalosyndactyly)--observations on a British series of thirty-nine cases. Ann Hum Genet Lond 24:151–164.

Chen L, Li D, Li C, Engel A, Deng C. 2003. A Ser250Trp substitution in mouse fibroblast growth factor receptor 2 (Fgfr2) results in craniosynostosis. Bone 33:169–178.

Cohen M. 2000. Apert syndrome. In: Cohen M, MacLean R, editors. Craniosynostosis: diagnosis, evaluation, and management. New York: Oxford University Press. p 316–353.

Cohen M, Kreiborg S. 1990. The central nervous system in the Apert syndrome. Am J Med Genet 35:36–45.

Cohen M, Kreiborg S. 1991. Agenesis of the corpus callosum. Its associated anomalies and syndromes with special reference to the Apert syndrome. Neurosurg Clin N Am 2:565–568.

Cohen M, Kreiborg S. 1993. An updated pediatric perspective on the Apert syndrome. Am J Dis Child 147:989–993.

Cohen M, Kreiborg S. 1994. Cranial size and configuration in the Apert syndrome. J Craniofac Genet Dev Biol 14:153–162.

Cohen M, MacLean R, editors. 2000. Craniosynostosis: diagnosis, evaluation, and management. New York: Oxford University Press. 454 p.

Cohen M, Kreiborg S, Lammer E, Cordero J, Mastroiacovo P, Erickson J, Roeper P, Martinez-Frias M. 1992. Birth prevalence study of the Apert syndrome. Am J Med Genet 42:655–659.

Darroch J, Mosimann J. 1985. Canonical and principal components of shape. Biometrika 72:241–252.

de Leon G, de Leon G, Grover W, Zaeri N, Alburger P. 1987. Agenesis of the corpus callosum and limbic malformation in Apert syndrome (type I acrocephalosyndactyly). Arch Neurol 44:979–982.

Eswarakumar V, Monsonego-Ornan E, Pines M, Antonopoulou I, Morriss-Kay G, Lonai P. 2002a. The IIIc alternative of Fgfr2 is a positive regulator of bone formation. Development 129:3783–3793.

Eswarakumar VP, Monsonego-Ornan E, Pines M, Antonopoulou I, Morriss-Kay GM, Lonai P. 2002b. The IIIc alternative of Fgfr2 is a positive regulator of bone formation. Development 129:3783–3793.

Falsetti A, Jungers W, Cole TR. 1993. Morphometrics of the callitrichid forelimb: a case study in size and shape. Int J Primatol 14:551–572.

Frinchi M, Bonomo A, Trovato-Salinaro A, Condorelli D, Fuxe K, Spampinato M, Mudò G. 2008. Fibroblast growth factor-2 and its receptor expression in proliferating precursor cells of the subventricular zone in the adult rat brain. Neurosci Lett 447:20–25.

Gagan J, Tholpady S, Ogle R. 2007. Cellular dynamics and tissue interactions of the dura mater during head development. Birth Defects Res C Embryo Today 81:297–304.

Gault D, Renier D, Marchac D, Jones B. 1992. Intracranial pressure and intracranial volume in children with craniosynostosis. Plast Reconstr Surg 90:377–381.

Gosain A, McCarthy J, Glatt P, Staffenberg D, Hoffmann R. 1995. A study of

intracranial volume in Apert syndrome. Plast Reconstr Surg 95:284–295.
Hill CA, Reeves RH, Richtsmeier JT. 2007. Effects of aneuploidy on skull growth in a mouse model of Down syndrome. J Anat 210:394–405.
Hughes S. 1997. Differential expression of the fibroblast growth factor receptor (FGFR) multigene family in normal human adult tissues. J Histochem Cytochem 45:1005–1019.
Iseki S, Wilkie AO, Morriss-Kay GM. 1999. Fgfr1 and Fgfr2 have distinct differentiation- and proliferation-related roles in the developing mouse skull vault. Development 126:5611–5620.
Lajeunie E, Cameron R, El Ghouzzi V, De Parseval N, Journeau P, Gonzales M, Delezoide A-L, Bonaventure J, LeMerrer M, Renier D. 1999. Clinical variability in patients with Apert's syndrome. J Neurosurg 90:443–447.
Lefebvre A, Travis F, Arndt E, Munro I. 1986. A psychiatric profile before and after reconstructive surgery in children with Apert's syndrome. Br J Plast Surg 39:510–513.
Lele S, Richtsmeier J. 2001. An invariant approach to the statistical analysis of shapes. London: Chapman and Hall/CRC Press.
Mann H, Whitney D. 1947. On a test of whether one of two random variables is stochastically larger than the other. Ann Math Stat 18:50–60.
Maric D, Pla A, Chang Y, Barker J. 2007. Self-renewing and differentiating properties of cortical neural stem cells are selectively regulated by basic fibroblast growth factor (FGF) signaling via specific FGF receptors. J Neurosci 27: 1836–1852.
Marsh J, Galic M, Vannier M. 1991. Surgical correction of the craniofacial dysmorphology of Apert syndrome. Clin Plast Surg 18:251–275.
Moss M. 1979. Functional cranial analysis and the functional matrix. Int J Orthod 17:21–31.
Moss M. 1997a. The functional matrix hypothesis revisited. 1. The role of mechanotransduction. Am J Orthod Dentofacial Orthop 12:8–11.
Moss M. 1997b. The functional matrix hypothesis revisited. 2. The role of an osseous connected cellular network. Am J Orthod Dentofacial Orthop 112:221–226.
Moss M. 1997c. The functional matrix hypothesis revisited. 3. The genomic thesis. Am J Orthod Dentofacial Orthop 112:338–342.
Moss M. 1997d. The functional matrix hypothesis revisited. 4. The epigenetic antithesis and the resolving synthesis. Am J Orthod Dentofacial Orthop 112: 410–417.
Moss M, Young R. 1960. A functional approach to craniology. Am J Phys Anthropol 18:281–202.
Noetzel M, Marsh J, Palkes H, Gado M. 1985. Hydrocephalus and mental retardation in craniosynostosis. J Pediatr 107:885–892.
Opperman L, Sweeney T, Redmon J, Persing J, Ogle R. 1993. Tissue interactions with underlying dura mater inhibit osseous obliteration of developing cranial sutures. Dev Dyn 198:312–322.
Opperman L, Passarelli R, Morgan E, Reintjes M, Ogle R. 1995. Cranial sutures require tissue interactions with dura mater to resist osseous obliteration in vitro. J Bone Miner Res 10:1978–1987.
Opperman L, Chhabra A, Nolen A, Bao Y, Ogle R. 1998. Dura mater maintains rat cranial sutures in vitro by regulating suture cell proliferation and collagen production. J Craniofac Genet Dev Biol 18:150–158.
Ornitz DM, Itoh N. 2001. Fibroblast growth factors. Genome Biol 2:1–12.
Ornitz D, Marie P. 2002. FGF signaling pathways in endochondral and intramembranous bone development and human genetic disease. Genes Dev 16: 1445–1465.
Parsons T, Ryan T, Reeves R, Richtsmeier J. 2007. Micro-structure of trabecular bone in a mouse model for Down syndrome. Anat Rec 290:414–421.
Passos-Bueno M, Sertie A, Jehee F, Fanganiello R, Yeh E. 2008. Genetics of craniosynostosis: genes, syndromes, mutations and genotype-phenotype correlations. In: Rice D, editor. Craniofacial sutures. Development, disease and treatment. Basel: Karger. p 107–143.
Patton M, Goodship J, Hayward R, Lansdown R. 1988. Intellectual development in Apert's syndrome: a long term follow up of 29 patients. J Med Genet 25: 164–167.
Pooh R, Nakagawa Y, Pooh K, Nakagawa Y, Nagamachi N. 1999. Fetal craniofacial structure and intracranial morphology in a case of Apert syndrome. Ultrasound Obstet Gynecol 13:274–280.
Posnick J, Armstrong D, Bite U. 1995. Crouzon and Apert syndromes: intracranial volume measurements before and after cranio-orbital reshaping in childhood. Plast Reconstr Surg 96: 539–548.
Quintero-Rivera F, Robson C, Reiss R, Levine D, Benson C, et al. 2006. Intracranial anomalies detected by imaging studies in 30 patients with Apert syndrome. Am J Med Genet 140A:1337–1338.
Renier D, Arnaud E, Cinalli G, Sebag G, Zerah M, Marchac D. 1996. Prognosis for mental function in Apert's syndrome. J Neurosurg 85:66–72.
Renier D, Lajeunie E, Arnaud E, Marchac D. 2000. Management of craniosynostoses. Childs Nerv Syst 16:645–658.
Richtsmeier JT, Paik C, Elfert P, Cole T, Dahlman HR. 1995. Precision, repeatability and validation of the localization of cranial landmarks using computed tomogrphay scans. Cleft Palate Craniofac J 32:217–227.
Richtsmeier J, Cole Tr, Krovitz G, Valeri C, Lele S. 1998. Preoperative morphology and development in sagittal synostosis. J Craniofac Genet Dev Biol 18: 64–78.
Richtsmeier J, Aldridge K, DeLeon V, Panchal J, Kane A, Marsh J, Yan P, Cole Tr. 2006. Phenotypic integration of neurocranium and brain. J Exp Zool B Mol Dev Evol 306:360–378.
Robb R, Hanson D, Karwoski R, Larson A, Workman E, Stacy M. 1989. ANALYZE: a comprehensive, operator-interactive software package for multidimensional medical image display and analysis. Comput Med Imaging Graph 13:433–454.
Slaney S, Oldridge M, Hurst J, Morriss-Kay G, Hall C, Poole M, Wilkie A. 1996. Differential effects of FGFR2 mutations on syndactyly and cleft palate in Apert syndrome. Am J Hum Genet 58:923–932.
Tokumaru A, Barkovich A, Ciricillo S, Edwards M. 1996. Skull base and calvarial deformities: association with intracranial changes in craniofacial syndromes. AJNR Am J Neuroradiol 17:619–630.
Tolarova M, Harris J, Ordway D, Vargervik K. 1997. Birth prevalence, mutation rate, sex ratio, parents' age, and ethnicity in Apert syndrome. Am J Med Genet 72:394–398.
Wang Y, Xiao R, Yang F, Karim B, Iocovelli A, Cai J, Lerner C, Richtsmeier J, Leszl J, Hill C, Yu K, Ornitz D, Elisseeff J, Huso D, Jabs E. 2005. Abnormalities in cartilage and bone development in the Apert syndrome FGFR2(+/S252W) mouse. Development 132:3537–3548.
Wang Y, Sun M, Uhlhorn V, Peter I, Hill C, Percival C, Richtsmeier J, Huso D, Jabs E. (in press). Activation of p38 MAPK pathway in the skull abnormalities of Apert syndrome Fgfr2+/P253R mice. BMC Dev Biol.
Wang H, Owens JD, Shih JH, Li MC, Bonner RF, Mushinski JF. 2006. Histological staining methods preparatory to laser capture microdissection significantly affect the integrity of the cellular RNA. BMC Genomics 7:97.
Wilke T, Gubbels S, Schwartz J, Richman J. 1997. Expression of fibroblast growth factor receptors (FGFR1, FGFR2, FGFR3) in the developing head and face. Dev Dyn 210:41–52.
Yacubian-Fernandes A, Palhares A, Giglio A, Gabarra R, Zanini S, et al. 2004. Apert syndrome: analysis of associated brain malformations and conformational changes determined by surgical treatment. AJNR J Neuroradiol 31:116–122.
Yacubian-Fernandes A, Palhares A, Giglio A, Gabarra R, Zanini S, et al. 2005. Apert syndrome: factors involved in the cognitive development. Arq Neuropsiquiatr 63:963–968.
Yin L, Du X, Li C, Xu X, Chen Z, Su N, Zhao L, Qi H, Li F, Xue J, Yang J, Jin M, Deng C, Chen L. 2008. A Pro253Arg mutation in fibroblast growth factor receptor 2 (Fgfr2) causes skeleton malformation mimicking human Apert syndrome by affecting both chondrogenesis and osteogenesis. Bone 42:631–643.